Feedforward and output–feedback control of the cell distribution in chemostat yeast fermentations ⋆

P. Jerono * **A. Schaum** * **T. Meurer** *

* *Automation and Control Group, Faculty of Engineering, Kiel University, Kiel, Germany, {pj,alsc,tm}@tf.uni-kiel.de*

Abstract: A two–degree–of–freedom control strategy is developed and experimentally validated for a set-point change along a desired trajectory of the cell distribution in yeast fermentation. Based on a mathematical model of yeast growth and cell population dynamics, an inversion–based feedforward controller is designed, utilizing a transformation between the biomass concentration and the cell distribution at the equilibrium points. To take disturbances and model inaccuracies into account, the controller is extended by a feedback control law. The controller is applied to a lab–scale stirred tank reactor with *Saccharomyces cerevisiae*.

Keywords: Cell population balance models, partial integro–differential equation, yeast fermentation, process control, tracking control.

1. INTRODUCTION

The control of cell population distributions in bioreactors is of particular interest when it comes to maintaining product quality or ensuring cell viability. The combination of feedforward and feedback control has turned out to be a robust strategy for set–point changes along a desired trajectory (Graichen et al., 2006; Schaum and Meurer, 2015; García-Sandoval et al., 2016; Schaum et al., 2017). The calculation of the feedforward signal is usually related to inverting the model equations and thus can rise in complexity when more detailed models are considered (Chen and Paden, 1996). Classical mass balance models of bioreactors are usually described by a set of ordinary differential equations (Schügerl and Bellgardt, 2000), whereas the modelling of cell population balances is more involved and typically leads to a partial integro–differential equation, which is coupled with a set of ordinary differential equations (Tsuchiya et al., 1966; Villadsen, 1999; Mhaskar et al., 2002; Daoutidis and Henson, 2002). Taking model and parameter uncertainties into account, which are usually present in biological processes, and in order to ensure robustness of the control strategy, it is advantageous to extend the feedforward controller by a feedback control law leading to the so called two–degree–of–freedom control (Horowitz, 2013). In process applications feedback controllers are typically designed by considering either direct output– or state–feedback control. In (Schaum et al., 2011, 2013) a model-free feedback controller is presented, which is motivated in its structure by a passive state–feedback control and leads to an equivalent PI controller with observer-based anti–windup protection. The suitability of this control approach for biological reactors has been experimentally validated in (García-Sandoval et al., 2016; Schaum et al., 2017).

⋆ Funded by the Deutsche Forschungsgemeinschaft (DFG, German Research Foundation) – Project-ID 395461267.

Having these results as points of departure, in this work a two–degree–of–freedom controller is designed for a set–point change of the cell mass distribution density function in the framework of an early lumping approach. It is shown that for every stationary biomass value there exists a unique stationary cell distribution. Exploiting this fact, and the relative degree of one for a pointwise output of the cell mass distribution density function and the internal stability property, a passivity–based two–degree–of–freedom control approach with model–free output–feedback control is designed and experimentally validated in an anaerobic continuous yeast fermentation experiment.

The paper is organized as follows. In Section 2 the cell population balance model is described. In Section 3 the equilibrium points of the lumped model are characterized. This is followed in Section 4 by an analysis of the structural controllability. The controller design is addressed in Section 5. The experimental setup is described in Section 6 and the obtained validation results discussed in Section 7. Conclusions are summarized in Section 8.

2. MODEL DESCRIPTION

Yeast growth follows the three substantial pathways

$$S + a_1 O_2 \xrightarrow{\rho_1} g_1 B + c_1 CO_2 \tag{1a}$$

$$S \xrightarrow{\rho_2} c_2 CO_2 + g_2 B + d_2 E \tag{1b}$$

$$E + a_3 O_2 \xrightarrow{\rho_3} g_3 B + c_3 CO_2, \tag{1c}$$

where B, S, E, O_2 and CO_2 denote the biomass, glucose, ethanol, oxygen, and carbon dioxide compounds respectively. The reaction rates of the metabolism pathways are given by ρ_i and the related stoichiometric coefficients are denoted by a_i, g_i and d_i, with $i \in \{1, 2, 3\}$. Reaction (1a) describes the oxidation of glucose to biomass, reaction (1b) the anaerobic production of ethanol and biomass and reaction (1c) represents the oxidation of ethanol to

biomass. Usually these reaction rates are chosen to capture characteristic effects of yeast growth like the crabtree effect (Deken, 1966). When considering anaerobic growth of yeast, only reaction (1b) takes place and the reaction dynamics can be described by a Monod growth rate

$$\rho(s) = k_s \frac{s}{s + K_s}, \tag{2}$$

where s denotes the glucose concentration, k_s is the maximum growth rate, and K_s is the half saturation constant.

2.1 Mass balance model

Based on the reaction scheme for anaerobic yeast growth in a chemostat reactor the following set of ordinary differential equations for the mass balance can be derived

$$\dot{b} = g_2\rho(s)b - Db, \qquad b(0) = b_0 \tag{3a}$$
$$\dot{s} = -\rho(s)b + D(s_{\text{in}} - s), \qquad s(0) = s_0, \tag{3b}$$

where b and s denote the concentrations of biomass and glucose, respectively. The glucose concentration in the inlet is given by s_{in} and D denotes the dilution rate, i.e., the quotient of in–/outflow and the reactor liquid volume. Note that in (3) the differential equation for ethanol production has been neglected, since ethanol will not be further considered, which is due to an anaerobic growth restriction.

2.2 Cell population balance model

The mass balance is complemented by the general cell population balance model (Villadsen, 1999; Mhaskar et al., 2002; Daoutidis and Henson, 2002; Mantzaris and Daoutidis, 2004) in chemostat operation mode

$$\begin{aligned}\partial_t n(m,t) = &-g_2\partial_m[r(m,s)n(m,t)]+\\ &-[\Gamma(m,s)+D]n(m,t)+\\ &+2\int_m^{m_*}\Gamma(\mu,s)p(m,\mu)n(\mu,t)\mathrm{d}\mu\end{aligned} \tag{4a}$$

$$\dot{s}(t) = -\int_0^{m_*} r(m,s)n(m,t)\mathrm{d}m + D(s_{\text{in}} - s) \tag{4b}$$

$$\begin{aligned}&n(m_*,t) = 0\\ &n(m,0) = n_0(m), \quad s(0) = s_0,\end{aligned} \tag{4c}$$

with $m \in [0, m_*]$ being the cell mass, m_* the maximum cell mass, t the time, $n(m,t)$ the cell mass distribution density at mass m at time t, $r(m,s)$ the cell growth rate function for mass m and substrate concentration s, $\Gamma(m,s)$ the associated cell division rate, $p(m,\mu)$ the partition probability density function determining the probability that by division of a mother cell of mass μ a daughter cell of mass m is produced. Note that in virtue of its definition, p has the property that

$$\forall \mu \le m: \quad p(m,\mu) = 0 \tag{5}$$

and is chosen as a symmetric binomial distribution (Mantzaris and Daoutidis, 2004)

$$p(m,\mu) = \frac{1}{B(q)}\frac{1}{\mu}\left(\frac{m}{\mu}\right)^{q-1}\left(1-\frac{m}{\mu}\right)^{q-1},$$

with the normalization factor

$$B(q) = \frac{2\Gamma_f(q)}{\Gamma_f(2q)},$$

where $\Gamma_f(\cdot)$ denotes the Gamma–function. Next a linear dependency of $r(m,s)$ on the cell mass m, as discussed in (Mantzaris and Daoutidis, 2004), is considered

$$r(m,s) = \rho(s)m. \tag{6}$$

Moreover the cell division rate $\Gamma(m,s)$ is assumed to be proportional to the cell growth rate

$$\Gamma(m,s) = \gamma(m)r(m,s). \tag{7}$$

The function $\gamma(m)$ is chosen to be a ramp function

$$\gamma(m) = \begin{cases} 0, & \text{if } m \le m^* \\ \beta(m-m^*), & \text{if } m^* < m, \end{cases} \tag{8}$$

where m^* is the minimal cell mass required for division and β is given by a constant. Note that the existence, uniqueness and positivity of solutions in $L^1 \times \mathbb{R}_+$ for (4) has been shown in (Beniich et al., 2018). The first moment of the cell population mass distribution density function is given by

$$b(t) = \int_0^{m_*} mn(m,t)\mathrm{d}m. \tag{9}$$

Recalling mass conservation during cell division (Mantzaris and Daoutidis, 2004; Schaum and Jerono, 2019), one obtains

$$\begin{aligned}\dot{b}(t) &= g_2\rho(s)\int_0^{m_*} mn(m,t)\mathrm{d}m - D\int_0^{m_*} mn(m,t)\mathrm{d}m\\ &= g_2\rho(s)b - Db\end{aligned} \tag{10a}$$

$$\begin{aligned}\dot{s}(t) &= -\rho(s)\int_0^{m_*} mn(m,t)\mathrm{d}m + D(s_{\text{in}} - s)\\ &= -\rho(s)b + D(s_{\text{in}} - s),\end{aligned} \tag{10b}$$

which corresponds to the mass balance model (3a) and (3b), so that both models are connected via the first moment of the cell mass distribution density function.

2.3 Discretized model equations

For the design of a controller in the framework of an early lumping approach and in virtue of its real–time implementation on a process control system, the cell population partial integro–differential equation (4) is discretized with respect to the mass domain. For this purpose, the partial derivative is approximated using the backwards finite differences scheme and the integral term is approximated using the trapezoidal rule. The discretized model equations are then given by

$$\begin{aligned}\dot{n}_i = &-\frac{1}{\Delta m}g_2\rho(s)(m_i n_i - m_{i-1}n_{i-1}) - [\Gamma(m_i,s)+D]n_i+\\ &+2\Delta m\sum_{j=i+1}^{z}\Gamma(m_j,s)p(m_i,m_j)n_j\end{aligned} \tag{11a}$$

$$\dot{s} = -\rho(s)b + D(s_{\text{in}} - s) =: f_s(D,\boldsymbol{x}) \tag{11b}$$

$$\begin{aligned}&n(m_{z+1},t) = 0\\ &n(m,0) = n_0(m), \quad s(0) = s_0,\end{aligned} \tag{11c}$$

where Δm is given by the discretization step size and z is the number of interior discretization points. Introducing the state vector $\boldsymbol{x}_n = [\boldsymbol{n}^T, s]^T = [n_1, \dots, n_z, s]^T$ equations (11) can be re–cast into the form

$$\dot{\boldsymbol{x}}_n = \boldsymbol{f}_n(D,\boldsymbol{x}_n) = \begin{bmatrix} A(D,s)\boldsymbol{n} \\ f_s(D,\boldsymbol{x}) \end{bmatrix}, \ \boldsymbol{x}(0) = \boldsymbol{x}_0 \in \mathbb{R}^{z+1} \tag{12}$$

with $A(s,D)$ being constructed from (11a) having an upper diagonal matrix structure with additional elements

on the lower diagonal originating from the backwards finite differences. Note that the boundaries of the cell distribution $n(0,t)$ and $n(m_*,t)$ can be excluded from the state vector, because $\rho(s)m_{\min}=0$ and $n(m_*,t)=0$. By this the approximated biomass b using the trapezoidal rule reads

$$b \approx \Delta m \sum_{i=1}^{z} m_i n_i. \tag{13}$$

3. EQUILIBRIUM POINTS IN CHEMOSTAT

For the simple mass balance model (3) it is well known that in a chemostat reactor in steady–state it holds that $D^* = g_2\rho(s^*)$ with the equilibrium points b^* and s^* given by (Schügerl and Bellgardt, 2000; Schaum et al., 2011)

$$b^* = g_2(s_{\text{in}} - s^*), \qquad s^* = \frac{D^* K_s}{g_2 k_s - D^*}. \tag{14}$$

Considering the cell population balance model (11) the equilibrium points can be calculated by solving the transformed system equations

$$\begin{bmatrix}\mathbf{0}\\ 0\end{bmatrix} = \begin{bmatrix} TA(D^*,s^*)\boldsymbol{n}^* \\ -\rho(s^*)b^* + D^*(s_{\text{in}} - s^*)\end{bmatrix} \tag{15}$$

$$T = \begin{bmatrix} \Delta m m_1 & \Delta m m_2 & \dots & \Delta m m_z \\ 0 & 1 & \dots & 0 \\ \vdots & \vdots & \ddots & \vdots \\ 0 & 0 & \dots & 1 \end{bmatrix} \tag{16}$$

which leads to

$$\begin{aligned} s^* &= \frac{D^* K_s}{g_2 k_s - D^*} \\ n_i^* &= \theta_i(n_z^*) \\ \theta_i(n_z^*) &= \frac{\theta_{i+1}(n_z^*)\left(\frac{g_2 m_{i+1}}{\Delta m} + m_{i+1}\gamma(m_{i+1}) + g_2\right)}{\frac{1}{\Delta m} g_2 m_i} \\ &\quad - \frac{2\Delta m \sum_{j=i+2}^{z} m_j \gamma(m_j) p(m_{i+1}, m_j)\theta_j(n_z^*)}{\frac{1}{\Delta m} g_2 m_i} \\ \theta_z(n_z^*) &= n_z^* \\ n_z^* &= \zeta^{-1}(s^*, n_z^*) \\ \zeta(s^*, n_z^*) &= -\rho(s^*)\Delta m \sum_{i=1}^{z} m_i \theta_i(n_z^*) + D^*(s_{\text{in}} - s^*). \end{aligned}$$

It can be seen that the solution of n_i^* only depends on the functions $\gamma(m)$, $p(m,\mu)$ and the value of g_2. Furthermore, by recursion, the solution of n_i^* can be expressed as a function of n_z^* and the value of n_z^* can be calculated based on the substrate dynamics by means of $\zeta^{-1}(s^*, n_z^*)$. This means that for every $i = 1,\dots,z$ there exists a linear (and thus invertible) transformation Φ_i such that $b^* = \Phi_i(n_i^*)$. Note that by this transformation the problem formulation of controlling the number of cells with specific mass can be rewritten in terms of biomass concentration.

To analyse if the equilibrium solution is locally stable, the eigenvalues $\boldsymbol{\lambda}$ of the linearized system are numerically determined and visualized for $D^* = 0.3\,\text{h}^{-1}$ and $D^* = 0.2\,\text{h}^{-1}$ which is shown in Fig. 1. It can be seen that all eigenvalues are located in the complex left half plane, i.e., the solution is locally asymptotically stable.

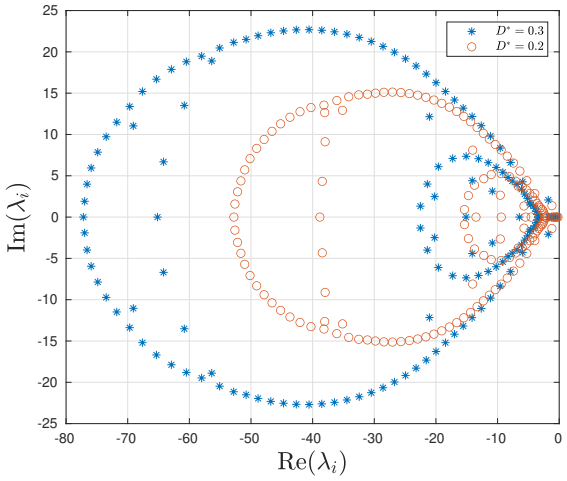

Fig. 1. Eigenvalues of the linearized system in equilibrium at $D^* = 0.3\,\text{h}^{-1}$ (blue stars) and $D^* = 0.2\,\text{h}^{-1}$ (red circles) with $z = 150$.

4. CONTROLLABILITY ANALYSIS

The controllability analysis of the model equations (11) is an involved task, because it usually relies on the calculation of Lie–derivatives up to a high order. In this work the structural controllability is analyzed by a graph–theoretical approach (Lin, 1974; Liu et al., 2011), where the calculation of Lie–derivatives can be avoided by only analysing the interconnections of the system states. In return, this analysis does not give any insight to the loss of the controllability property due to unfavourable parameters in the model equations. The network graph of the

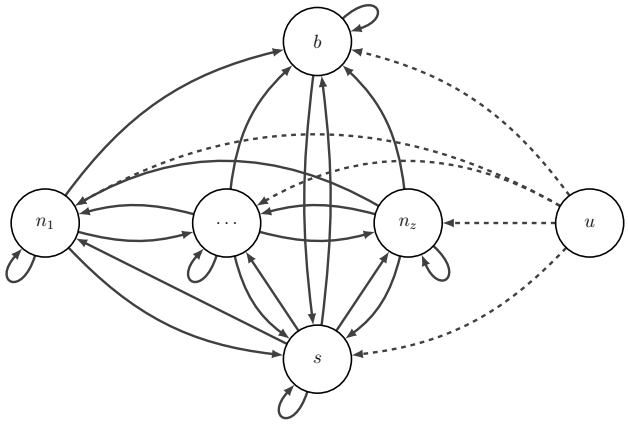

Fig. 2. Network graph of the system equations (11).

model equations (11) is shown in Fig. 2. Without the input node u the network graph is already strongly connected, i.e., from two distinct nodes i and j there exist a path $i \to j$ and $j \to i$ through the network. Additionally all system states are self–edged nodes. These facts allow to exclude the existence of inaccessibility and dilation (Liu et al., 2011). Therefore an arbitrary node of the network could be chosen as the driver (or leader) node. The interconnections from the input u to the system states are given by the dashed lines. It can be seen that every system state has an interconnection to the input, meaning that each state

is influenced by the input, which in the considered SISO-case corresponds to a relative degree of one for every node. Thus any chosen driver node can be modified by the input and therefore the system is structurally controllable.

5. CONTROLLER DESIGN

In this section a two–degree–of–freedom control strategy is developed for a set–point change of the cell distribution along a desired trajectory.

5.1 Feedforward controller

In order to determine the corresponding input trajectory for a given desired state trajectory $\boldsymbol{x}_d$, one would have to invert the system dynamics, i.e.,

$$u_d = D_d = \boldsymbol{f}_n^{-1}(\boldsymbol{x}_d) \tag{17}$$

which again is an involved task. The previous analysis of the equilibrium points revealed that there exists a unique transformation $b^* = \Phi_i(n_i^*)$ for all $i = 1, \ldots, z$. According to the controllability analysis, an arbitrary node of the system can be chosen to design the feedforward controller. This allows to design the desired trajectory for the cell distribution and transform it to the corresponding biomass concentration such that the feedforward input signal can be determined based on inverting the mass balance model (3), which is a much easier task. Note that this requires that the cell population dynamics are sufficiently fast for small changes in the dilution rate, which at this point is an assumption. The desired trajectory $n_d(t)$ for a given point $d \in \{1, \ldots, z\}$ is chosen to be

$$n_d(t) = n_{d,0} + (n_{d,T} - n_{d,0}) \left[3 \left(\frac{t}{T} \right)^2 - 2 \left(\frac{t}{T} \right)^3 \right], \tag{18}$$

where T is the final transition time and $n_{d,0}$ is the initial value of n at $m = m_d$, and $n_{d,T}$ the desired final value. The desired trajectory is then transformed to the corresponding biomass values

$$b_d(t) = \Phi_d(n_d(t)). \tag{19}$$

The input signal can finally be calculated by

$$D_d(t) = g_2 \rho(s_d(t)) - \frac{\dot{b}_d(t)}{b_d(t)}, \tag{20}$$

where $s_d(0)$ is determined from (14) and $s_d(t)$ is obtained by substituting (20) in (3b) and solving the obtained differential equation numerically.

5.2 Feedback controller

In order to take model uncertainties, approximation errors or parameter offsets into account and to ensure robustness against process disturbances it is advantageous to extend the feedforward controller by an stabilizing feedback control law. In this work the model–free approach employed in (Gonzalez and Alvarez, 2005; Diaz-Salgado et al., 2012; García-Sandoval et al., 2016; Schaum et al., 2017) is considered. Since the feedforward controller is reformulated in terms of biomass concentrations, which is an on–line measurement at our reactor by means of optical density, it is also possible to design the feedback controller in terms of biomass concentrations. For this consider the variables

$$\tilde{y} = y - y_d, \quad \tilde{D} = D - D_d, \quad y_d = h(\boldsymbol{x}_d) = b_d \tag{21}$$

and the error dynamics of the mass balance model (3)

$$\begin{aligned} \dot{\tilde{y}} &= g_2 \rho(s) b - D b - g_2 \rho(s_d) b_d + D_d b_d =: \Psi(\boldsymbol{x}, D) \\ \tilde{y}(0) &= \tilde{y}_0. \end{aligned} \tag{22}$$

The error dynamics can be rewritten as the feedback interconnection

$$\dot{\tilde{y}} = -\alpha \tilde{D} + v \tag{23a}$$

$$v = \alpha \tilde{D} + \Psi(\boldsymbol{x}, D) =: \nu(\boldsymbol{x}, D) \tag{23b}$$

with the weighting factor $\alpha \neq 0$. According to the constructive control approach (Sepulchre et al., 2012) a stabilizing passivity-based state-feedback controller is given by

$$\tilde{D} = \frac{\kappa \tilde{y} + v}{\alpha} = \tilde{\omega}(\tilde{y}, v), \quad v = \nu(\boldsymbol{x}, D). \tag{24}$$

With the assumption that the function $\nu(\boldsymbol{x}, D)$ is slowly time varying compared to a time–scale ω^{-1} of an appropriately parameterized observer, the value of v can be estimated by

$$\dot{\hat{v}} = -\omega(\hat{v} - (\dot{\tilde{y}} + \alpha \tilde{D})). \tag{25}$$

In terms of the estimated state

$$\chi = \hat{v} - \omega \tilde{y} \tag{26}$$

the dynamics (25) can be rewritten as

$$\dot{\chi} = -\omega \chi - \omega(\omega \tilde{y} - \alpha \tilde{D}), \quad \hat{v} = \chi + \omega \tilde{y}. \tag{27}$$

Utilizing the estimate $\hat{v}$ in (24) and considering controller saturation by means of $\tilde{D}^+$ and $\tilde{D}^-$ (which are functions of D_d) the output–feedback tracking controller is given by

$$\dot{\chi} = -\omega \chi - \omega(\omega \tilde{y} - \alpha \tilde{D}), \quad \hat{v} = \chi + \omega \tilde{y} \tag{28a}$$

$$\tilde{D} = \begin{cases} \tilde{D}^+, & \tilde{\omega}(\tilde{y}, \hat{v}) > \tilde{D}^+ \\ \tilde{\omega}(\tilde{y}, \hat{v}), & \tilde{D}^- \leq \tilde{\omega}(\tilde{y}, \hat{v}) \leq \tilde{D}^+ \\ \tilde{D}^-, & \tilde{\omega}(\tilde{y}, \hat{v}) < \tilde{D}^- \end{cases}. \tag{28b}$$

For implementation purposes, following (Schaum et al., 2017) $\alpha = b_d$ is chosen, which leads to a time–varying weighting in the feedback controller (24). As shown in (Schaum et al., 2011, 2013) the resulting controller can be rewritten in terms of a saturated PI control scheme (with time–varying gain).

Note that the feedback controller could also be constructed based on the cell population density function, which (for our reactor setup) would require the design of an appropriate state observer. The structural observability property of the system (11) for available biomass measurements is derived in (Jerono et al., 2021a) together with the design of an extended Kalman Filter, that can be implemented in parallel for process monitoring purposes.

6. EXPERIMENTAL SETUP

A yeast fermentation chemostat experiment was carried out in a 2 liter stirred–tank reactor. The process conditions are listed in Table 1. To ensure that the yeast growth process is performed under anaerobic conditions the reactor is aerated with nitrogen, such that ethanol will only be produced as a byproduct and can be neglected in the model description. Optical density measurements are taken on–line at 750 nm wavelength with a sample time of 1 second. Cell distribution measurements are taken at discrete time steps with a Casy Cell Counter and Analyser.

The parameters of the cell population balance model are determined to fit the experimental data from previous experiments. A detailed explanation of the parameter identification process of the presented cell population balance model can be found in (Jerono et al., 2021b). The complete set of model parameters is listed in Table 2. Note that the

Table 1. Process conditions

Parameter	Value	Unit
Temperature	25	°C
Aeration (N_2)	0.10	vvm
controlled pH	5.5	-
Stirrer speed	750	rpm
Glucose (s_{in})	9.2	g/l

Table 2. Model parameter

Parameter	Value	Unit
k_s	2.9660	h^{-1}
K_s	0.7000	gS/l
g_2	0.1847	gB/gS
q	5.0000	-
m^*	$5.4808 \cdot 10^{-11}$	g
m_*	$1.5000 \cdot 10^{-10}$	g
β	$1.2142 \cdot 10^{21}$	-

parameter values listed in Table 2 slightly differ to those presented in (Jerono et al., 2021b), which is due to recent adaptations in the process and reactor setup.

7. RESULTS

The results of the proposed two–degree–of–freedom control in a yeast fermentation chemostat experiment are presented in Fig. 3 to Fig. 6. For the parameterization of the feedback controller (28) $\omega = 0.1\,\text{h}^{-1}$ and $\kappa = 1.5\,\text{h}^{-1}$ are chosen. The transition time is fixed to $T = 5\,\text{h}$ and the initial and final states in (18) are chosen as $n_{d,0} = 8.992 \cdot 10^{20}\,\#/\text{g/l}$ and $n_{d,T} = 9.435 \cdot 10^{20}\,\#/\text{g/l}$ with $d = 15$ and $m_d = 4.327 \cdot 10^{-11}\,\text{g/l}$, leading to $b_{d,0} = 1.61\,\text{g/l}$ and $b_{d,T} = 1.69\,\text{g/l}$. The transition between two operation points is carried out two times. First from the initial to the final operation point according to (18) and in the second step a transition back to the initial operation point is realized, by switching $n_{d,0}$ and $n_{d,T}$. In Fig. 3 the desired biomass trajectory (red), the on–line measurement (blue) and the estimation of an extended Kalman Filter (EKF) (yellow) are shown. In Fig. 4 the feedforward signal and the applied input are presented and a significant mismatch between both signals can be observed. This can be attributed to a required higher dilution rate for stabilizing the initial equilibrium point in the experiment, which is due to the presence of perturbations and model inaccuracies. These facts motivate the combination of a feedforward and feedback controller. In Fig. 5 snapshots of the cell distribution density function are presented, where the continuous (red) line in time shows the desired trajectory $n_d(t)$. In Fig. 6 the measurement are evaluated at the cell mass of $m = 4.33 \cdot 10^{-11}\text{g/l}$. At each measurement time instance of the cell distribution three samples are taken and for each sample three measurement cycles are performed, which leads to overall nine distribution measurements. The y_1 (green), y_2 (blue) and y_3 (purple) signals correspond to the average

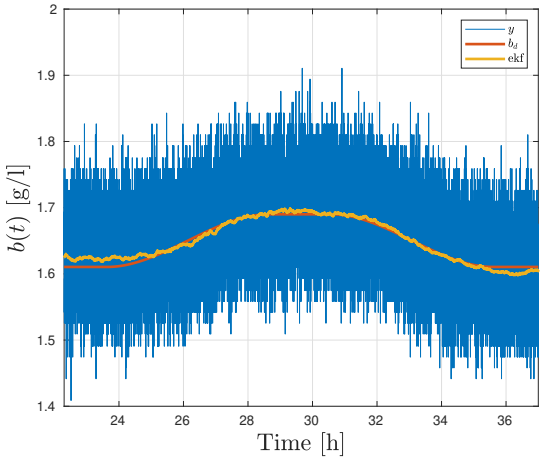

Fig. 3. Biomass in the experiment. Measurement y (blue), desired b_d (red) and estimated by EKF (yellow).

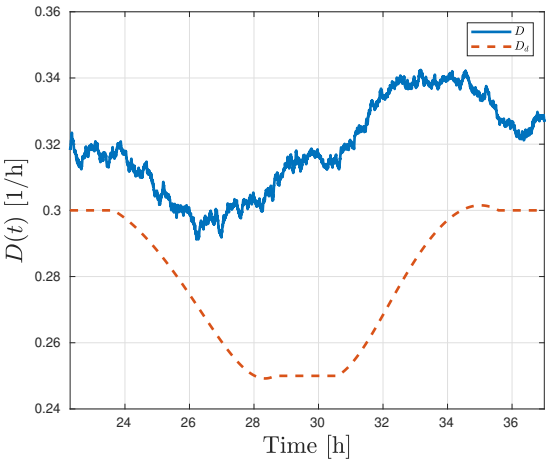

Fig. 4. Input in the experiment. Feedforward D_d (dashed-red) and two–degree–of–freedom controller D (blue).

of three measurements for each taken sample. Comparing these signals a high spread can be recognized, which can be explained by the high dilution factors required for the measurements and small measurement deviations in each sample. Therefore all taken measurements have been averaged once more leading to $\bar{y}$ (filled–black) in Fig. 6 which show a good agreement with the desired trajectory. The experimental results support the assumption from Section 5 that for small changes in the dilution rate the cell population dynamics are sufficiently fast.

8. CONCLUSION

A two–degree–of–freedom controller for the transition between operation points of a chemostat bioreactor with respect to the cell number of a specific mass along a desired trajectory is designed. Based on the analysis of the equilibrium points and the structural controllability of the cell population balance model the problem formulation can be rewritten in terms of biomass concentrations. Finally the controller is validated in an experimental setup showing a good agreement of the desired and measured trajectory.

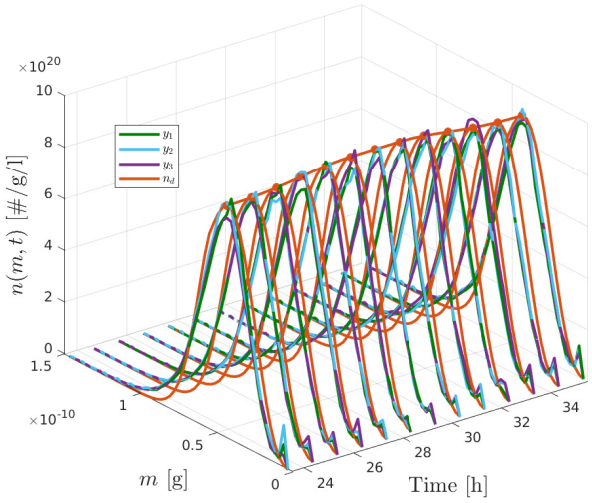

Fig. 5. Cell distribution density function measurements from three samples y_1, y_2 and y_3 (green, blue and purple) and desired trajectory n_d (continuous–red).

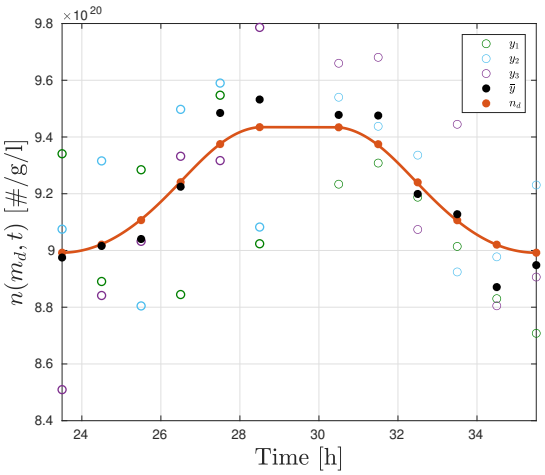

Fig. 6. Cell density measurements at the desired mass. Measurements from three samples y_1, y_2 and y_3 (green, blue and purple), average value (black) and desired trajectory n_d (continuous–red).

REFERENCES

Beniich, N., Abouzaid, B., and Dochain, D. (2018). On the existence and positivity of a mass structured cell population model. Appl. Math. Sci., 12 (19), 921–934.

Chen, D. and Paden, B. (1996). Stable inversion of nonlinear non-minimum phase systems. International Journal of Control, 64(1), 81–97.

Daoutidis, P. and Henson, M. (2002). Dynamics and control of cell populations in continuous bioreactors. AIChe Symposium Series, 326, 274–289.

Deken, R.H.D. (1966). The Crabtree Effect: A Regulatory System in Yeast. Microbiology, 44(2), 149–156.

Diaz-Salgado, J., Alvarez, J., Schaum, A., and Moreno, J.A. (2012). Feedforward output-feedback control for continuous exothermic reactors with isotonic kinetics. Journal of Process Control, 22(1), 303–320.

García-Sandoval, J., Méndez-Acosta, H., González-Álvarez, V., Schaum, A., and Alvarez, J. (2016). VFA robust control of an anaerobic digestion pilot plant: experimental implementation. IFAC-PapersOnLine, 49, 973–977.

Gonzalez, P. and Alvarez, J. (2005). Combined PI-inventory control of solution homo- polymerization reactors. Ind. Eng. Chem. Res. J., 44, 7147–7163.

Graichen, K., Hagenmeyer, V., and Zeitz, M. (2006). Feedforward control with online parameter estimation applied to the chylla–haase reactor benchmark. Journal of Process Control, 16, 733–745.

Horowitz, I.M. (2013). Synthesis of feedback systems. Elsevier.

Jerono, P., Schaum, A., and Meurer, T. (2021a). Moment-based Kalman filter design for cell population balance models in batch fermentation processes. IFAC-PapersOnLine, 54(3), 19–24.

Jerono, P., Schaum, A., and Meurer, T. (2021b). Parameter identification of a yeast batch cell population balance model. IFAC-PapersOnLine, 54(7), 144–149.

Lin, C.T. (1974). Structural controllability. IEEE Trans. Autom. Control., 19, 201–208.

Liu, Y.Y., Slotine, J.J., and Barabási, A.L. (2011). Controllability of complex networks. Nature, 473(7346), 167–173.

Mantzaris, N.V. and Daoutidis, P. (2004). Cell population balance modeling and control in continuous bioreactors. Journal Process Control, 14, 775–784.

Mhaskar, P., Hjortso, M.A., and Henson, M. (2002). Cell population modeling and parameter estimation for continuous cultures of saccharomyces cerevisiae. Biotechnol. Prog., 18, 1010–1026.

Schaum, A. and Jerono, P. (2019). Observability analysis and observer design for a class of cell population balance models. IFAC-PapersOnLine, 52(2), 189–194.

Schaum, A., Alvarez, J., and Lopez-Arenas, T. (2011). Saturated output-feedback control for a class of continuous fermenters. IFAC Proceedings Volumes, 44(1), 7126–7131.

Schaum, A., Alvarez, J., and Lopez-Arenas, T. (2013). Saturated linear dynamic output-feedback control for a class of three-state continuous bioreactors with inhibited kinetics. Journal of Process Control, 23(3), 332–350.

Schaum, A. and Meurer, T. (2015). Inversion-based feedforward control design for the droop model. Computer-Aided Chemical Engineering, 37, 1601–1606.

Schaum, A., Weisbarth, H., and Meurer, T. (2017). Robust adaptive feedforward output-feedback tracking control for microalgae cultures. IFAC-PapersOnLine, 50, 12667–12672.

Schügerl, K. and Bellgardt, K.H. (2000). Bioreaction Engineering. Springer Verlag.

Sepulchre, R., Jankovic, M., and Kokotovic, P.V. (2012). Constructive nonlinear control. Springer Science & Business Media.

Tsuchiya, H.M., Fredrickson, A.G., and Aris, R. (1966). Dynamics of Microbial Cell Populations. Advances in Chemical Engineering, 6(C), 125–206.

Villadsen, J. (1999). On the use of population balances. Journal of Biotechnology, 71, 251–253.